
Article:
Smith, PR, Cowell, DMJ and Freear, S (2013) Width-modulated square-wave pulses for ultrasound applications. IEEE Transactions on Ultrasonics, Ferroelectrics, and Frequency Control, 60 (11). 2244 - 2256. ISSN: 0885-3010

https://doi.org/10.1109/TUFFC.2013.6644730

Width-Modulated Square-Wave Pulses for Ultrasound Applications

Peter R. Smith, *Student Member, IEEE,* David M. J. Cowell and Steven Freear, *Senior Member, IEEE*

***Abstract*—A method of output pressure control for ultrasound transducers using switched excitation is described. The method generates width-modulated, square-wave pulse sequences that are suitable for driving ultrasound transducers using MOSFET devices or similar. Sequences are encoded using an optimized level-shifted, carrier-comparison, pulse-width modulation (PWM) strategy derived from existing PWM theory, and modified specifically for ultrasound applications. These modifications are: a reduction in carrier frequency so that the least amount of pulses are generated and minimal switching is necessary; alteration of a linear carrier form to follow a trigonometric relationship in accordance with the expected fundamental output; and application of frequency modulation to the carrier when generating frequency modulated, amplitude tapered signals.**

The PWM method permits control of output pressure for arbitrary waveform sequences at diagnostic frequencies (approximately 5 MHz) when sampled at 100 MHz, and is applicable to pulse shaping and array apodization. Arbitrary waveform generation capability is demonstrated in simulation using convolution with a transducer's impulse response, and experimentally with hydrophone measurement. Benefits in coded imaging are demonstrated when compared with fixed-width square-wave (pseudo-chirp) excitation in coded imaging, including reduction in image artifacts and peak sidelobe levels for two cases, showing 10 dB and 8 dB reduction in peak sidelobe level experimentally, compared to 11 dB and 7 dB reduction in simulation with the Field II package. In all cases the experimental observations correlate strongly with simulated data.

I. Introduction

An ultrasound system uses a transducer to convert electrical signals into pressure waves which propagate through a medium, such as human tissue, and reflect back towards the transducer when encountering an impedance mismatch. The transducer converts the reflected pressure waves into electrical signals that are captured and processed to enable non-invasive measurement or imaging. Imaging transducers often contain arrays of elements, each of which ideally requires a transmitter circuit for greatest flexibility, thus necessitating an array of transmitter circuits. Advances in areas of ultrasound such as high frequency imaging [1] and portable, low-cost system development [2], [3], place a burden on the complexity and requirements of an ultrasound transmitter, particularly when the design is required to be scaled over many channels. Complexity may also increase as future trends seek to integrate excitation electronics into the transducer probe head which has a number of benefits, including improved impedance matching and reducing the unwieldy cable bundle between system and probe [4].

High frequency linear power amplifiers are well-suited to the electrical requirements of ultrasound transmitters, however are often large, bulky and expensive components. An alternative transmitter solution to linear power amplifiers is the use of MOSFET semi-conductor pulser devices. These components use switched excitation to select between several positive and negative voltage levels. Switching between discrete levels results in square-wave or staircase (stepped) pulses which approximate sinusoidal signals as described in [1]–[11]. MOSFETs are advantageous particularly over linear power amplifiers as they are capable of delivering high currents to piezo-electric loads [12], in small scale, low-cost, integrated packages and are more suited for use with arrays of channels. The nature of MOSFET switched excitation often results in pulses with uniform fixed amplitude. Whilst it is possible to adjust switching levels between firings, it is often desirable to control pulse amplitude throughout the duration of the excitation for several applications within therapeutic and diagnostic ultrasound.

An example application that requires amplitude control, or arbitrary waveform capability is transmit array apodization. This technique is known to improve diagnostic imaging, by reducing pressure around the mainlobe, thus lowering scattering from targets outside the intended beam. Array apodization requires a different amplitude weighting to be applied to each element [13], [14], thus requiring per-element transmit flexibility. A second example application includes coded imaging - an established technique of increasing SNR in ultrasound systems which has been well discussed in previous literature such as [15] and set of papers [16]–[18]. In general, the technique relies upon the correlation between the transmitted pulse and received signal to distinguish between low intensity echoes generated by weak scatterers and the ambient noise floor. Most often, linear frequency modulated (LFM) signals are chosen over phase modulated signals as they do not require multiple transmissions and do not contain abrupt changes in phase. In the case of frequency modulated signals, the embedded 'code' is the rate of the increase (or decrease) from a start frequency to the stop frequency, over time. Frequency Modulated coded transmissions benefit greatly from amplitude tapering at the start and end of the pulse. This technique therefore requires a transmitter capable of generating frequency modulated transmission signals and applying a desired tapering function.

Pulse width modulation (PWM) is an established technique used throughout engineering to control switched mode output. In its simplest form, the duty cycle or on/off ratio of a square wave is adjusted in proportion to a desired, time-averaged

The authors are with the Ultrasound Group, School of Electrical and Electronic Engineering, University of Leeds, Leeds, LS2 9JT, UK, e-mail: efy3prs@leeds.ac.uk, s.freear@leeds.ac.uk. The work was supported by the Engineering and Physical Sciences Research Council (EPSRC).

Manuscript received X X, XXXX; revised X X, XXXX.

output. PWM has a wide range of applications due to its relatively low cost, ease of implementation and high efficiency. Previous literature has described adjusting switching thresholds (and hence pulse widths) of square wave pulses to eliminate harmonics in the transmitted output [8]. The objective of [8] was not to control pulse shape or amplitude however, but to reduce harmonic content. A recent paper [11] discussed the advantages of MOSFET bipolar pulsers, particularly with respect to the large amplitude outputs available, but dismissed the use of MOSFETs for generating arbitrary excitation, stating a lack of control over pulse characteristics. In contrast, authors such as Persson have previously described varying the width and shape of very short square-wave pulses to effect the transmitted pressure output [19] which showed potential for amplitude control. It is the objective of this work to investigate the use of PWM strategies for ultrasound applications, thus providing control of pulse characteristics and arbitrary waveform capability, using high-voltage switched-mode sequences.

There are many forms and implementations of PWM, particularly in power converters where a wealth of literature is available as summarized in [20]. For ultrasound applications a number of aspects differ from conventional implementations. Traditional PWM strategies use a multitude of pulses to describe the modulating waveform. This requires rapid switching of the transmitter circuit at a rate much greater than the output frequency and is often used in combination with an output filter [21]. This form of rapid switching and reconstruction is similar to a sigma-delta modulation strategy as proposed by Huang and Li [22]. A sigma-delta implementation generates multiple switching events in response to an integration stage operating on a sample by sample basis. The train of pulses are time-averaged over the duration of the half cycle, with the density of the pulses defining the resultant output amplitude. Consequently, for low- or mid-amplitude signals, multiple sparsely distributed pulses are generated with durations that are very small. The technique proposed in this work differs, as it seeks to minimize the number of switching events to one pulse per half cycle as in a pseudo-chirp representation, but modulate the width of each of the pulses in the sequence. Widths are modulated by using the characteristics of the transducer as a bandpass filter and considering the transducer's response to a square-wave input. The transducer's bandwidth is of key importance, as it's frequency response restricts which frequencies within a square-wave are transmitted into the medium. The PWM method described provides a solution to address the reported inflexibility of high voltage bipolar pulser devices for generation of windowed or arbitrary waveforms, as described in recent literature such as [10] and [11].

The paper is structured as follows: Section II discusses a simple form of PWM sequence generation using a carrier based comparison method [23]. Modifications to the conventional carrier are described to make the output suitable for ultrasound with an adjusted algorithm defined. Section III demonstrates how pressure control can be obtained using the PWM strategy with potential applications in both diagnostic and therapeutics. Section IV further modifies the carrier to accommodate frequency modulated sequences, with improvements in coded imaging demonstrated using PWM to apply pulse tapering as described by [16], [17]. The paper ends with a discussion of the method and a summary of conclusions.

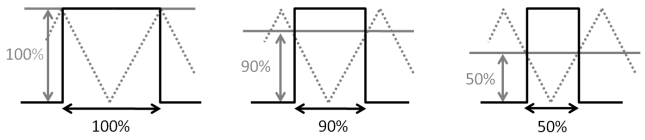

Fig. 1. Examples of Triangular (sawtooth) Symmetrical Pulse Width Modulation. Consisting of a carrier (dotted line), and a desired output level (grey solid line). A comparison algorithm using the carrier and a desired level, generating a width modulated pulse (black solid line). The triangular form of the carrier generates symmetrically modulated PWM with both the leading-edge, and trailing-edge of the square-wave modulated.

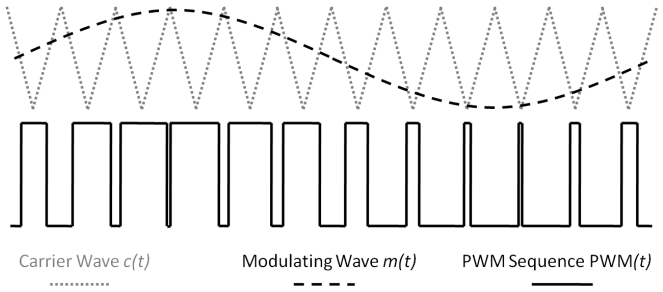

Fig. 2. Diagram of conventional carrier-based PWM featuring the carrier $c(t)$ and modulating wave $m(t)$.

II. PWM and Multilevel PWM

A. Overview of carrier-based PWM

Conventional carrier-based PWM compares a carrier of known form to a desired output level or modulating wave thus generating pulses of varying widths [23]. Fig. 1 shows three examples of modulation with an often-used triangular carrier generating three symmetrically modulated pulses after comparison with desired d.c voltage levels.

The conventional triangular carrier assigns a pulse width from a desired output level in a linear fashion. The width of the pulse is therefore directly proportional to the desired d.c. level. A linear triangular carrier may be defined as:

$$c(t) = A \cdot |(2/\pi)(\sin^{-1}(\sin(\omega t + \phi)))| + L \qquad (1)$$

where A is a scaling factor, t is time, ϕ is phase, L is an arbitrary d.c. offset and $\omega = 2\pi f$ with f representing frequency. The triangular carrier described by (1) can be used to modulate the widths of successive pulses by comparing said carrier to a modulating wave $m(t)$. With this method, the square wave is 'high' or 'on' whilst $c(t) < m(t)$. In most applications $m(t)$ is of much lower frequency than the carrier, resulting in multiple pulses of varying widths, with the ratio of carrier frequency to modulating frequency determining the number of pulses per cycle, as demonstrated in Fig. 2.

In digital implementations of PWM, both the carrier and modulating wave are discrete representations of a continuous signal. A second relationship then exists between $c(t)$, $m(t)$ and the overall sampling frequency f_s. For this work, due to the high frequency of the excitation signal to be described, a

single pulse per half cycle relationship was defined, resulting in two width-modulated (i.e. one positive and one negative) pulses for a single cycle. This reduces switching losses, lowers the required sampling frequency and relaxes the specification of the transmit output circuitry.

For ultrasound applications, and for a single half cycle square-wave pulse, it can be shown that whilst output pressure is proportional to the width of the pulse, it is not directly or linearly proportional to the width of the pulse. That is to say that a linear relationship between pulse width and pressure output does not exist, with a percentage increase in pulse width not providing the same percentage increase in output pressure. Therefore a triangular or sawtooth carrier as defined in (1) and shown in Fig. 1 and Fig. 2 is not appropriate. This can be explained by considering the transducer as a bandpass filter with a defined bandwidth within which it is sensitive to a particular range of frequencies. The resultant pressure wave can be modelled as a convolution between the input signal, and the impulse response of the transducer which has a defined bandwidth. Frequencies outside of the transducer's bandwidth are heavily attenuated with almost no out-of-band energy transmitted by the transducer through the medium. It is therefore the relationship between a linearly increasing pulse width, and the output magnitude of the frequencies within the transducer's bandwidth which must be considered.

The relationship between harmonic content and switching angle for square wave signals can be calculated using Fourier series analysis [21]. Fig. 3 shows a bipolar square wave with variable angle δ and Fourier series

$$f(t) = \frac{a_0}{2} + \sum_{n=1}^{\infty} (a_n \cos nt + b_n \sin nt) \tag{2}$$

$$a_0 = 0,$$

$$a_n = 0,$$

$$b_n = \frac{2V}{n\pi} \cos(n\delta) \left[1 - (-1)^n\right] \tag{3}$$

$$f(t) = \sum_{n=1}^{\infty} \left(\frac{2V}{n\pi} \cos(n\delta) \left[1 - (-1)^n\right] \sin nt \right) \tag{4}$$

where a_0, a_n and b_n are Fourier series coefficients, and a_0 and a_n are equal to zero due to a lack of d.c. component and rotational symmetry respectively, and V is the peak amplitude. If δ is varied linearly between 0 and $\pi/2$, then the magnitude of the b_n in (3) decreases as shown in Fig. 4 and described previously for power converters by Bedford and Hoft [21]. It can be seen from Fig. 4 that the relationship between a linearly increasing switching threshold or square wave pulse width, and the magnitude of harmonic component that the relationship between the pulse width and fundamental output is indeed not linear, but trigonometric.

If we consider that the magnitude of the fundamental is of most importance due to the influence of the transducer, then pulse widths must be assigned according to this relationship, and not using a linear carrier as discussed in conventional PWM. For carrier comparison PWM, this requires a change in carrier form.

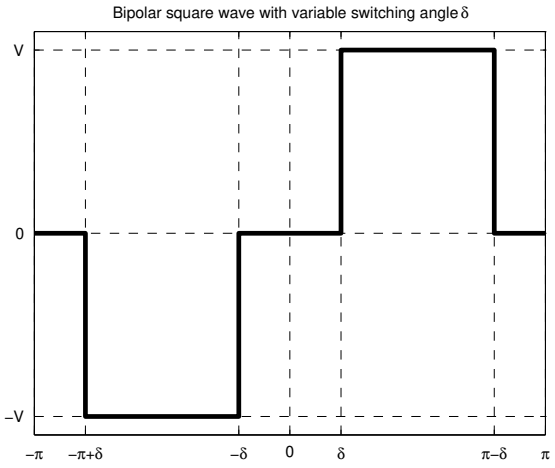

Fig. 3. Bipolar square wave with variation of switching angle δ

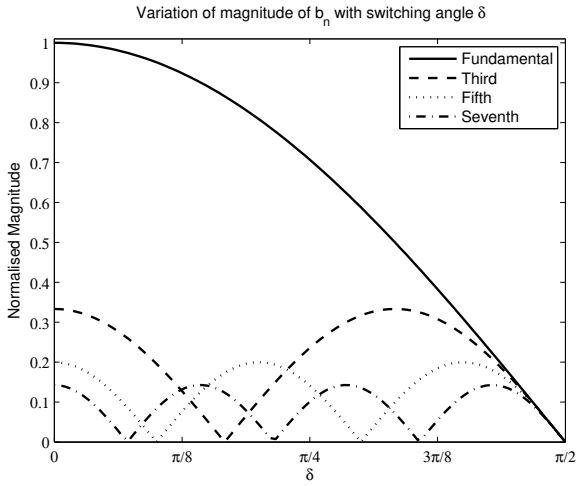

Fig. 4. Harmonic energy within a Pulse Width Modulated square wave of increasing width with switching angle. Absolute values are normalized to the fundamental [21].

B. Trigonometric Carrier Definition

Optimization of the carrier to provide a non-linear increase in pulse width for a linearly increasing desired output can be defined like so:

$$c(t) = A \cdot \mid \cos(\omega t + \phi) \mid + L \tag{5}$$

When the carrier defined by (5) is used in a carrier-comparison PWM method, symmetrically modulated PWM sequences are generated, with both the leading and trailing edges modulated simultaneously [23]. Fig. 5 demonstrates the difference between a traditional triangular carrier and the proposed trigonometric carrier, with both carriers scaled within the range $0 \leq c(t) \leq 1$.

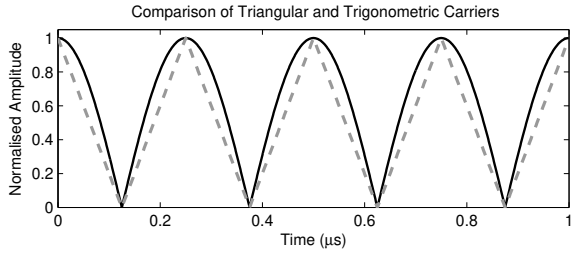

Fig. 5. Comparison of a triangular (grey dashed) vs a trigonometric (black solid) carrier.

C. Extension to Multiple Level PWM

Typically, several d.c. voltage levels are used to describe the desired excitation. Indeed the use of multiple level MOSFET switching circuits is commonplace for switching inverters [24] but also applies to ultrasound [10], [25]. The use of multiple levels is advantageous for PWM as it increases the number of available states with which to describe the desired amplitude, at a cost of increased hardware.

For multi-level carrier comparison PWM, strategies exist in power converter theory which are applicable to ultrasound. In the case of level-shifted carrier comparison PWM, each switching leg or MOSFET is assigned a carrier, with the carriers scaled to cover the defined region of switching, contiguous in amplitude, but with a d.c. offset [23] as described in (5). Examples of three-level and five-level carrier definitions using level-shifted carriers are shown in Fig. 6.

D. Generation of PWM Sequences

The carrier comparison methods generate PWM sequences using an algorithmic approach. It is therefore appropriate to first explain conventional algorithms as discussed in common literature before explaining the proposed algorithmic change. Therefore, bipolar (three-level) PWM sequences can be generated with two, level-shifted carriers and an algorithm as shown in (6).

$$\text{PWM}(t) = \begin{cases} 1, & m(t) \geq c_{\text{POS}}(t) \\ -1, & m(t) \leq c_{\text{NEG}}(t) \\ 0, & \text{otherwise} \end{cases} \tag{6}$$

where $m(t)$ is the modulating signal and $c_{\text{POS}}(t)$ and $c_{\text{NEG}}(t)$ are carriers which span the positive and negative regions respectively. This algorithm can then be extended for multiple levels by introducing additional carriers and levels as described by (7).

$$\text{PWM}(t) = \begin{cases} 1, & m(t) \geq c_{\text{POS2}}(t) \\ 0.5, & m(t) \geq c_{\text{POS1}}(t) \\ -1, & m(t) \leq c_{\text{NEG2}}(t) \\ -0.5, & m(t) \leq c_{\text{NEG1}}(t) \\ 0, & \text{otherwise} \end{cases} \tag{7}$$

where $c_{\text{POS1}}(t)$ and $c_{\text{POS2}}(t)$ are carriers that span the positive ranges between 0 to 0.5 and 0.5 to 1 respectively and $c_{\text{NEG1}}(t)$ and $c_{\text{NEG2}}(t)$ span the ranges between 0 to -0.5 and 0.5 to -1 respectively.

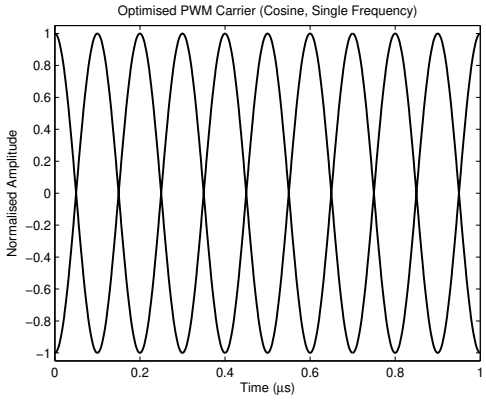

(a) Three-Level Single Frequency Optimised Carrier

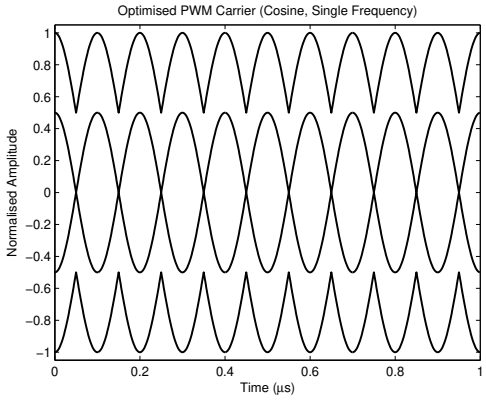

(b) Five-Level Single Frequency Rectified Cosine Carrier

Fig. 6. Carrier scaling for multi-level PWM generation using the proposed trigonometric carrier. The carrier is replicated a number of times, scaled and then level-shifted in order to span the range of the modulating signal $m(t)$

The algorithms described in (6) and (7) take a conventional low frequency signal and generate multiple pulses per cycle. For ultrasound, due to the high frequency output signal the proposed method modifies traditional algorithms to generate a single, width-modulated pulse per half cycle. The proposed algorithm compares two signals: a sinusoidal signal and a desired amplitude function with the carrier setup. Two versions of the desired amplitude function are created, the original which spans from 0 to 1, and the inverse from -1 to 0. The full algorithm is shown in (8):

$$\text{PWM}(t) = \begin{cases} \text{if} \quad s(t) \geq 0 & \\ \quad 1, & m_{\text{POS}}(t) \geq c_{\text{POS2}}(t) \\ \quad 0.5, & m_{\text{POS}}(t) \geq c_{\text{POS1}}(t) \\ \quad 0, & \text{otherwise} \\ \text{else} & \\ \quad -1, & m_{\text{NEG}}(t) \leq c_{\text{NEG2}}(t) \\ \quad -0.5, & m_{\text{NEG}}(t) \leq c_{\text{NEG1}}(t) \\ \quad 0, & \text{otherwise} \end{cases} \tag{8}$$

where $s(t) = A \cdot \sin(\omega t + \phi)$ and is scaled from -1 to 1, and where $m_{\text{POS}}(t)$ and $m_{\text{NEG}}(t)$ are positive and negative (or inverse) versions of the desired window function respectively. For clarity an example is shown in Fig. 7. In the proposed method, frequency information is within the carrier, with

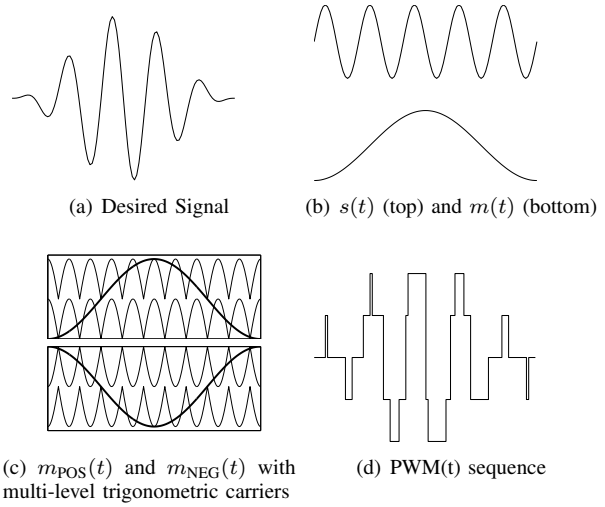

(a) Desired Signal (b) $s(t)$ (top) and $m(t)$ (bottom)

(c) $m_{\text{POS}}(t)$ and $m_{\text{NEG}}(t)$ with multi-level trigonometric carriers (d) PWM(t) sequence

Fig. 7. Example to show application of the algorithm to generate the proposed ultrasound sequences. The desired waveform 7(a) is a tone burst with an applied window function, and can be split into its constituent parts $s(t)$ and $m(t)$ as shown in 7(b). Using these constituent parts the carrier and positive and negative window functions are created 7(c). Using the sign of $s(t)$ comparison between either positive or negative aspects are performed to generate the resultant PWM sequence as shown in 7(d).

amplitude information stored within the modulating function.

III. Multilevel PWM for Pressure Amplitude Control

Using the algorithm defined in (8), multi-level arbitrary waveform sequences can be designed which give the desired output signal once filtered by a transducer. It is possible to simulate the filtering effect of the transducer by measuring its impulse response, and convolving this with the PWM signal. The simulated pressure output can then be compared with the measured output.

Fig. 8 shows an example arbitrary waveform sequence of a 4.8 MHz, 10 μs tone-burst with a desired linearly increasing ramp modulating function $m(t)$. Fig. 8(a) shows the generated PWM sequence derived using the process previously described. Fig. 8(b) shows a simulated output performed in MATLAB (Mathworks, Natick, MA) when the PWM sequence, designed using the proposed trigonometric carrier setup, is convolved with the measured impulse response of a linear array transducer (128 Elements, L3-8 40EP, Prosonic, Korea, 57% Average Bandwidth, Average Center Frequency 4.8 MHz). Fig. 8(c) shows the experimentally measured pressure wave obtained with a 1 mm needle hydrophone (Precision Acoustics, Dorset, UK) in counjunction with a LeCroy Waverunner 64xi digital oscilloscope (LeCroy Corporation, Chestnut Ridge, NY, USA). The transducer was excited with PWM sequences, uploaded to the UARP system (University of Leeds, Leeds, UK) [25], [26]. It can be seen that the simulated and experimentally obtained pressure outputs are closely matched, with a slight difference in peak positive and negative amplitudes seen due to non-linear propagation.

A second application that requires generation of sequences with amplitude control, such as that demonstrated in Fig. 8, is array apodization. Apodization across an array requires elements to be excited with signals of varying amplitude Fig. 9 shows a plot detailing PWM excitation sequences generated for apodization of an array aperture for linear imaging using a linear imaging transducer (128 Elements, L3-8 40EP, Prosonic,

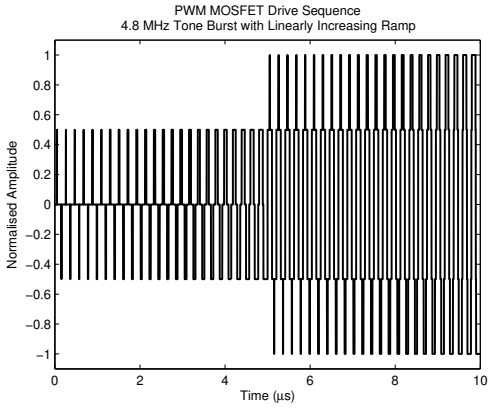

(a) Five-level PWM sequence

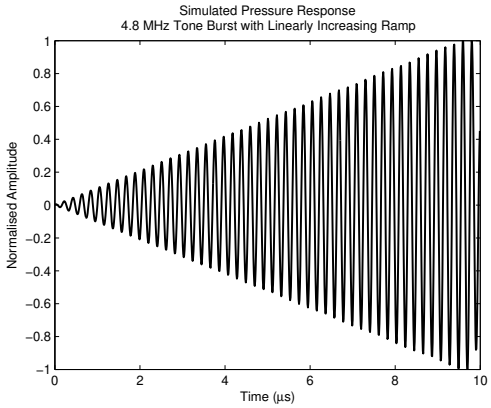

(b) Simulated pressure output

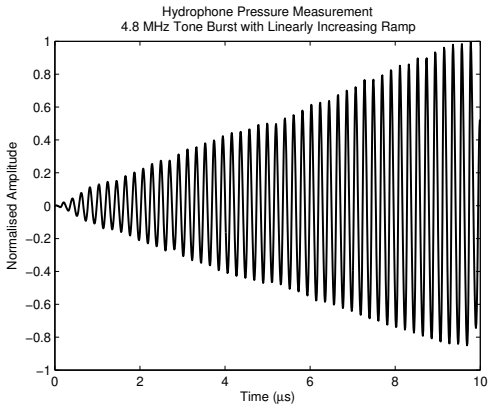

(c) Experimentally obtained pressure output

Fig. 8. Single frequency (4.8 MHz) 10 μs tone burst with linearly increasing amplitude function applied, sampled at f_s = 100 MHz. PWM Sequences are encoded using the proposed trigonometric carrier which assigns pulse widths in accordance to the expected response of the fundamental frequency when passed through the transducer. Simulation is obtained by convolving the PWM signal with the measured transducer impulse response. Experimental measurement is obtained using a needle hydrophone. It can be seen that the simulated and experimental results are closely matched.

Korea, 57% Average Bandwidth, Average Center Frequency 4.8 MHz), and also shaping of the transmitted pulse. In this example a 5-cycle, 5-MHz Gaussian windowed pulse has been designed with Gaussian apodization across an aperture of 48 elements Fig. 9(a). The ideal (truncated) Gaussian function is shown in Fig. 9(b) as well as a rectangular weighting function. Figs. 9(c) and 9(d) show Field II simulation, and experimental data respectively, comparing the unapodized case (rectangular - no aperture weighting) and the apodized case (Gaussian apodization obtained using the PWM strategy). Simulation using Field II allows the measured transducer response to be used during simulation, and also can take into account factors such as focal depth, aperture size and length of excitation sequence. Experimental measurements were obtained using the UARP system, in conjunction with a 0.2 mm hydrophone (Precision Acoustics, Dorset, UK), and a LeCroy WaveRunner 64xi Digital Oscilloscope. The experimental case is averaged over 50 acquisitions. Both simulated and experimental results show an expected reduction in sidelobe pressure, and slight widening of the mainlobe as a result of applied apodization. Differences between Figs. 9(c) and 9(d) can be attributed to simulation not accounting for non-linear propagation and formation of 'shock-waves', directivity of the needle hydrophone and the dynamic range of the 8-bit digital oscilloscope (8 bit, 48 dB) during signal acquisition.

The proposed PWM method enables shaping of pulses and output amplitude control using switched excitation as demonstrated in Figs. 8 and 9. The PWM method described can be used to modulate arbitrary pulse sequences by altering the designed amplitude function in accordance with the desired pulse shape. Pulse shaping is particularly important in coded imaging where it is advantageous to taper the pulse to suppress sidelobes. A more detailed explanation of the role of PWM in coded imaging is now discussed in Section IV.

IV. Multilevel PWM for use in Coded Imaging

Ultrasound coded imaging, as discussed by Misaridis and Jensen [16]–[18] is a technique that transmits a signal with an embedded feature or code, such as frequency modulation, that can be detected in the presence of noise. At the receiver, a 'pulse compression' filter is necessary to detect the coded signal and indicate correlation or a matched response. The pulse compression filter is also known as a matched filter. One optimal design for the matched filter is to use the inverse (or time-reversed, complex-conjugate) of the transmitted sequence [16], [17]. Tapering of the excitation pulse and applying a window to the filter can also provide additional benefits, as the nature of the taper or window function can offer gains in SNR at a cost of decreased axial resolution. This section aims to demonstrate the efficacy of the multi-level PWM discussed in the previous sections to accurately describe a number of tapering functions for use in coded ultrasound imaging.

A. Linear Frequency Modulated Chirp Design

Digitally generated LFM signals as described by Misaridis and Jensen in [17] equation (3) are defined as

$$s(t) = a(t) \cdot \exp\left\{ j2\pi \left[\left(f - \frac{B}{2} \right) t + \frac{B}{2T} t^2 \right] \right\} \quad (9)$$

$$\text{with } 0 \leq t \leq T$$

where B is the signal bandwidth, $a(t)$ is an applied window function or taper and the LFM signal sweeps from $f_{\text{START}} = f - B/2$ to $f_{\text{STOP}} = f + B/2$ in time T, at rate $k = B/T$ [17]. For signal detection, an appropriate pulse compression or matched filter is designed. The pulse compression filter demodulates the signal, with the output approximating a sinc function [17]. If no additional tapering or weighting is applied then the signal is said to have a rectangular window function. Rectangular window functions cause sidelobes at approximately -13.2 dB below the peak in the correlation output response as discussed by numerous authors [27]. Applying a window function to the match filter design, by altering $a(t)$ successfully reduces near sidelobes at a cost of widening the mainlobe. If a rectangular windowed signal is transmitted, and a window function applied to the match filter (now called a 'mis-matched filter') near sidelobe levels can be estimated as reported in [27]–[29].

The performance of the pulse compression system is also defined by the time-bandwidth product TB. For large TB values (i.e. exceeding 100) the performance of the system is similar to that discussed in coded radar literature [30]. In ultrasound however, the TB product is limited by the transducer's bandwidth, and the signal duration. It is therefore unusual to have very high TB products when imaging closely spaced targets, as their matched filter responses will overlap in time and frequency as discussed in [31]. Also, long duration sequences restrict imaging of targets very close to the transducer. For LFM signals with low TB products and rectangular window functions, their amplitude spectrum contains significant Fresnel ripples. These ripples cause distortion in the pulse compressed output referred to as far sidelobes that are not removed by the windowed matched filter. Indeed as reported by Misaridis "Amplitude tapering is the most efficient way to reduce the Fresnel ripples of the spectrum, if the power amplifier allows control of the transmitted pulse rise time" [17]. In this work, tapering of a frequency modulated excitation can be achieved by using the PWM strategy previously discussed, but with extension for use with LFM signals.

B. Windowing and Tapering Functions

The optimum for pulse compression is to taper the excitation signal to reduce Fresnel ripples and far sidelobes, and design a weighted matched (mis-matched) filter to reduce near sidelobes. When this is the case, the expected sidelobe level (ignoring the effect of the transducer) can be estimated by considering the frequency response of the product of the two time domain windowing functions. This differs from expected values reported in [27]–[29].

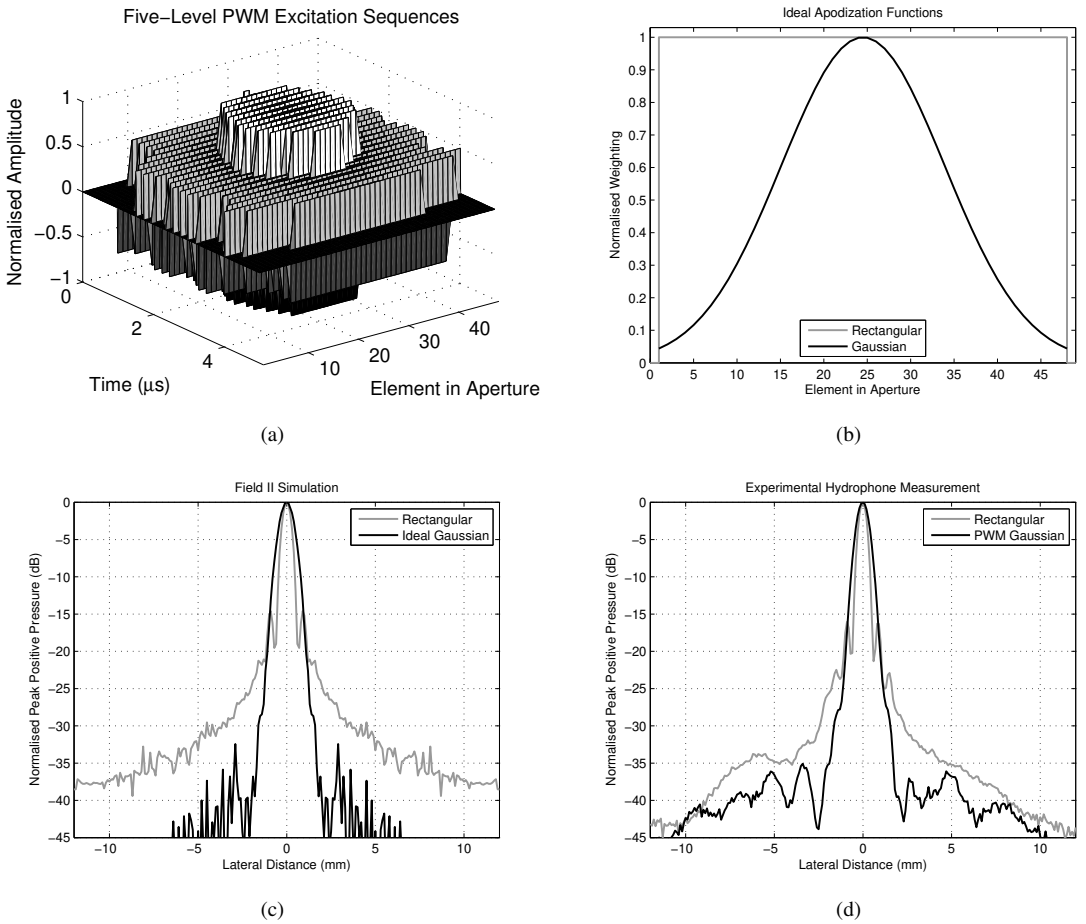

Fig. 9. Example of PWM encoded sequences for time tapering and array apodization. MOSFET drive sequences are encoded for 5 MHz, 5 cycle Gaussian-windowed excitations, with Gaussian array apodization over an aperture of 48 elements, Fig. 9(a). The ideal Gaussian function compared with a rectangular function is shown in Fig. 9(b). Field II simulation of the expected ultrasound field is shown in Fig. 9(c). Simulation and Experimental measurements show decreased sidelobe levels in the lateral beam plot at 30 mm focus when compared with a rectangular aperture with applied time tapering in both the ideal simulated case, and using the PWM strategy, Fig. 9(d).

C. Swept Frequency Level Shifted Carrier Comparison

The previous sections discussed generation of PWM sequences for amplitude control of single frequency tone-burst signals with a carrier-comparison method. The carrier comparison method requires a rectified, scaled and phase-shifted copy of the desired signal to be used as a carrier. Therefore to generate PWM sequences of LFM signals with defined bandwidth it is necessary to apply the same frequency modulation to the carrier signal. This ensures that a single, multi-level pulse per half cycle is generated at the correct position, is symmetrically modulated, and maintains frequency information. The frequency modulated carrier can therefore be seen as an extension of (5) and is defined as

$$c(t) = A \cdot \mid \cos(\omega\prime t + \phi) \mid + L \tag{10}$$

where $\omega\prime = 2\pi((f - \frac{B}{2}) + \frac{B}{2T})$, with B the bandwidth of the signal. Fig. 10 shows examples of the frequency modulated carrier arranged for generation of multi-level PWM sequences which can be used with (8) according to the following process:

- Generate a frequency modulated signal $s(t)$ of desired duration, center frequency and bandwidth.
- Define the carrier of same duration, center frequency, and bandwidth, but with a $\pi/2$ phase shift.
- Scale and level shift the carriers so they are contiguous and describe the range -1 to 1.
- Generate an appropriate excitation tapering function or time window, e.g. Hann, Hamming or Raised Cosine window as described in [27].
- Create positive and negative versions of the window function.
- Use the sign of $s(t)$ to switch alternately between comparisons of the positive window function to the positive carriers (when $s(t)$ is positive), to comparisons of the negative window function to the negative carriers (when $s(t)$ is negative).

V. LFM Chirp Coded Imaging

Examples of coded images using multi-level chirp coded PWM sequences are described in this section. The PWM sequences are encoded with the optimized frequency-modulated, rectified cosine carrier method described in Section IV. A wire phantom consisting of five, 0.125 mm diameter titanium wires, submerged in deionized degassed water and separated

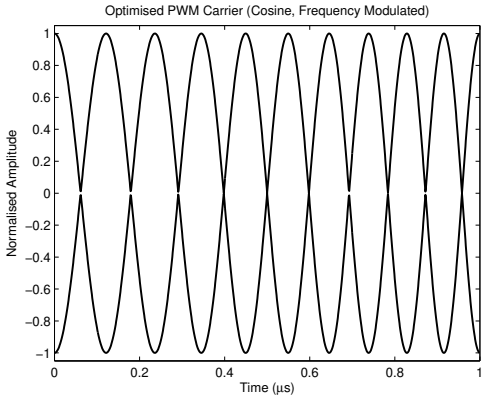

(a) Three-Level Swept Frequency Optimised Carrier

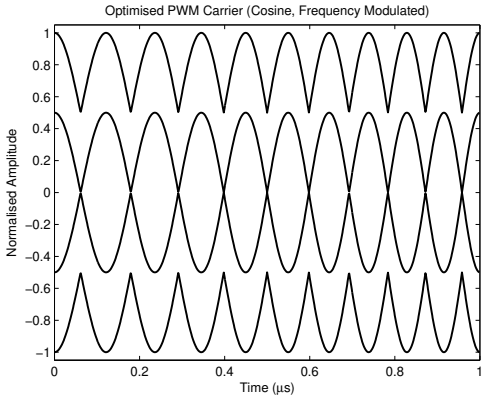

(b) Multi-Level Swept Frequency Rectified Cosine Carrier

Fig. 10. Linear frequency modulation of the carrier.

by 1.27 mm is constructed, and imaged with a medical array transducer (128 Elements, L3-8 40EP, Prosonic, Korea, 57% Average Bandwidth, Average Center Frequency 4.8 MHz) and the UARP system. Two examples of coded PWM signals with applied tapering functions have been designed and used to excite 96 elements of the medical imaging transducer following a standard linear imaging principle as described in [13]. An aperture of 48 elements is sequentially moved across 96 elements of the array transducer using the UARP system, with a focused beam (focal point 60 mm) transmitted toward the wire phantom. The focal point was chosen to be at the middle of the five wires. The same 48 elements of the aperture are used to receive echoes sampled at 50 MHz. The raw radio frequency data is then apodized and beamformed according to standard delay and sum principles to form a single line focused at 60 mm. A weighted pulse compression filter as described previously is then used for mismatched filtering. Two signals have been used in each chirp cases, firstly a fixed-width, square wave pseudo-chirp [5] [6] fluctuating between two levels (referred to as 'Bipolar (Fixed-Width)') and secondly a PWM chirp sequence encoded using five levels, using the trigonometric carrier setup as shown in Fig. 10, according to the algorithm described in (8). The bipolar 'fixed-width pseudo-chirp' $p(t)$ is defined using

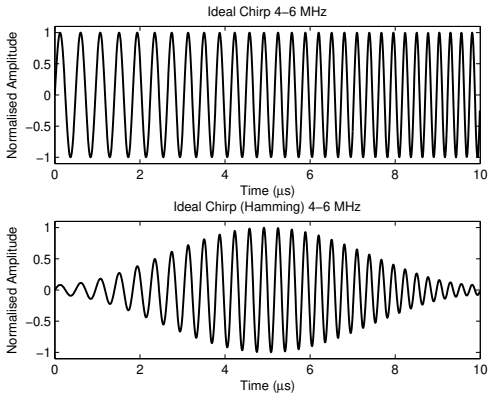

Fig. 11. Ideal 4-6 MHz chirp signals no window (top) and Hamming windowed (bottom) used as reference waveforms for the bipolar (fixed-width), and 5-level PWM-encoded signals. Chirp parameters: f = 5 MHz, $T = 10$ μs, $B = 2$ MHz, $TB = 20$, $k = 0.2$ MHz/μs.

$$p(t) = \begin{cases} 1 & \text{if } s(t) > 0, \\ -1 & \text{if } s(t) < 0, \\ 0 & \text{if } s(t) = 0, \end{cases} \tag{11}$$

where $s(t)$ is defined as per (9) but with $a(t)$ a constant value. Both signals are switched-mode square wave excitations which are subject to the bandpass characteristics of the transducer and have the same weighted mismatched filter applied. Any difference between sidelobe level or mainlobe width between the two signals is therefore as a result of excitation tapering.

Fig. 13 shows experimentally obtained images of the wire phantom plotted with a 45 dB dynamic range. Each of the five wires appear as bright spots. Only one of the wires appears at the focal point. Other wires that are not in focus appear blurred or spread laterally. The excitation signal used in this case is a 4-6 MHz Hamming windowed chirp of 5 MHz center frequency (f), 2 MHz bandwidth (B), 10 μs duration (T), TB =20, k =0.2 MHz/μs. Note that this bandwidth is within the reported 57% bandwidth of the transducer, which will also naturally taper the wide-bandwidth signal. Both switched excitation sequences (fixed-width and width modulated) have been generated with a 100 MHz sampling frequency. Note in the case of the 'fixed-width' case, the Hamming windowing does not apply. The corresponding 'ideal' chirps are shown in Fig. 11 with the corresponding bipolar and PWM encoded MOSFET gate drive-signals shown in Fig. 12. For the fixed-width pulse case shown in Fig. 13(a), high sidelobes are apparent in areas between wires. These appear as a lighter grey regions indicating sidelobes at -30 dB. When compared with the five-level PWM case 13(b), the sidelobes have been reduced, however the wire at the focal point (seen at approximately 65 mm in the reconstructed image) has been lengthened slightly. This is as a consequence of both the excitation taper and the filter windowing function as described in [17].

Sidelobe levels can be more accurately compared by plotting the central line of the image which intersects the five wires. As these images are produced using a single focus, it is appropriate to compare the single wire in the focal region.

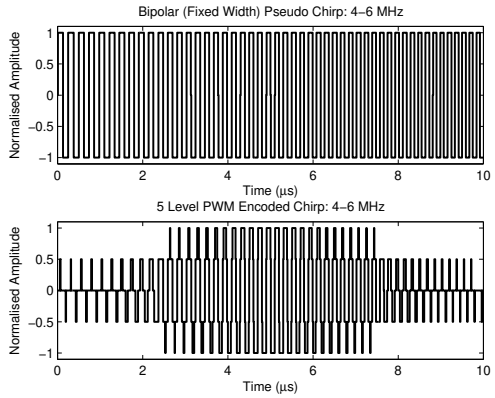

Fig. 12. MOSFET gate drive signals of the bipolar (fixed-width) 4-6 MHz chirp signal (top) and the 5-level PWM-encoded 4-6 MHz chirp signal (bottom).

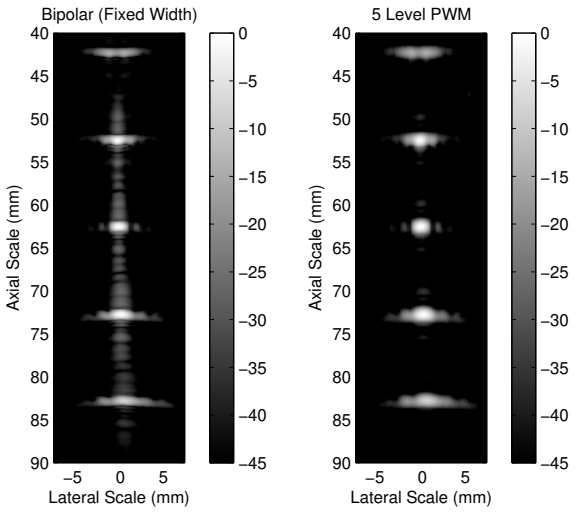

(a) (b)

Fig. 13. Experimental wire phantom coded images using the 'bipolar (fixed-width) pseudo-chirp' and PWM-encoded Hamming 4-6 MHz chirp signals.

Fig. 14 shows simulated and experimental results of the image center line, showing the wire at the focal point. Simulations are performed in MATLAB using the ultrasound simulation toolbox, Field II [32], [33]. Care has been taken to ensure that the simulation environment is as close to the experimental environment as possible, with the measured transducer impulse response used in simulation. Analysis of Fig. 14 shows an expected improvement of 11 dB in peak sidelobe level when using the PWM signals according to simulation (-26 dB to -37 dB), with an experimentally observed improvement of 10 dB (-26 dB to -36 dB) in peak sidelobe level. Also noticeable is an increase in mainlobe width for the PWM case as a consequence of the applied tapering function.

Fig. 17 shows a second example of experimentally obtained images of the wire phantom using the same array transducer as the previous case. The excitation signal used in this case is a Hamming windowed 3-6 MHz chirp of 4.8 MHz center frequency (f), 2.88 MHz bandwidth (B), and 10 μs duration (T), TB =28.8, k =0.288 MHz/μs. This value of bandwidth

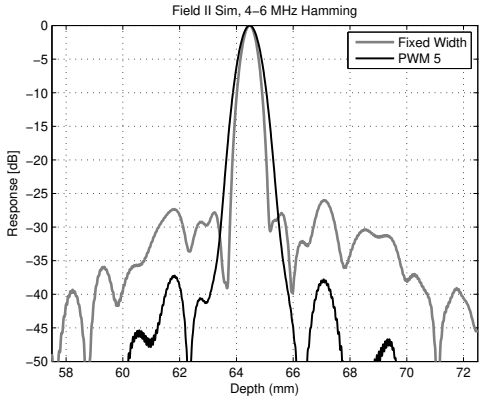

(a) Simulation

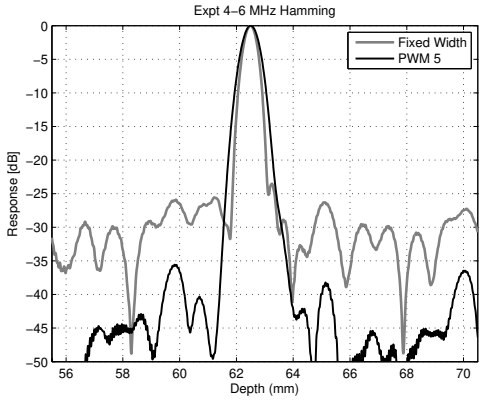

(b) Experimental

Fig. 14. Center line plotted limited to view a single wire at the focal point. Simulated data in the Fig. 14(a). Experimentally obtained in Fig. 14(b).

was chosen to match the reported bandwidth of the L3-8 40EP transducer (57%) around its peak frequency. Note that as this bandwidth is at the edge of the transducer's bandwidth, both signals, including the bipolar (fixed width) case will undergo amplitude tapering at low and high bandwidths. The ideal chirps are shown in Fig. 15 with the corresponding MOSFET drive signals shown in Fig. 16. Note that as per the previous case, the bipolar fixed-width case does not have the Hamming windowing applied. It can again be seen that the sidelobes in the region between targets are reduced when comparing the fixed-width sequence to the PWM sequences.

Fig. 18 shows simulated and experimental results of the image center line, showing the wire at the focal point. In this case simulation predicts an improvement in peak sidelobe level when using PWM sequences of approximately 7 dB (-30 dB to -37 dB), with experimental measurement showing an improvement in 8 dB (-30 dB to -38 dB). Also noticeable, when compared with the previous case in Fig. 14 is a slight increase in axial resolution as a result of increased bandwidth. In the case of the PWM results, the mainlobe width is increased slightly due to amplitude tapering.

VI. Discussion

Sections III and IV have shown that the carrier modifications and algorithm proposed is suitable for applications

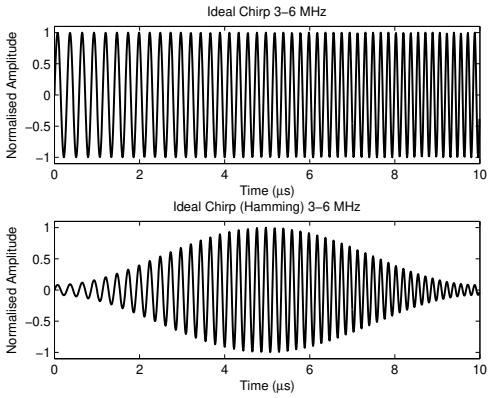

Fig. 15. Ideal 3-6 MHz chirp signals no window (top) and Hamming windowed (bottom) used as reference waveforms for the bipolar (fixed-width), and 5-level PWM-encoded signals. Chirp parameters: f = 4.8 MHz, $T = 10$ μs, $B = 2.88$ MHz, $TB = 20$, $k = 0.288$ MHz/μs.

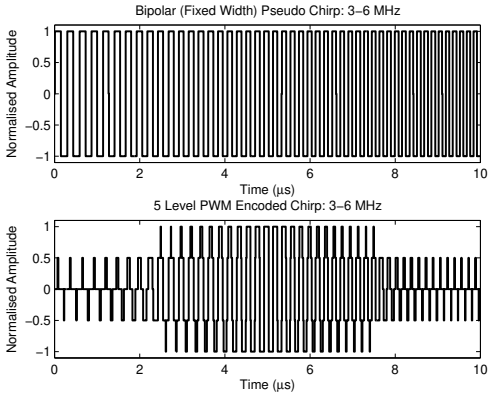

Fig. 16. MOSFET gate drive signals of the bipolar (fixed-width) 3-6 MHz chirp signal (top) and the 5-level PWM-encoded 3-6 MHz chirp signal (bottom).

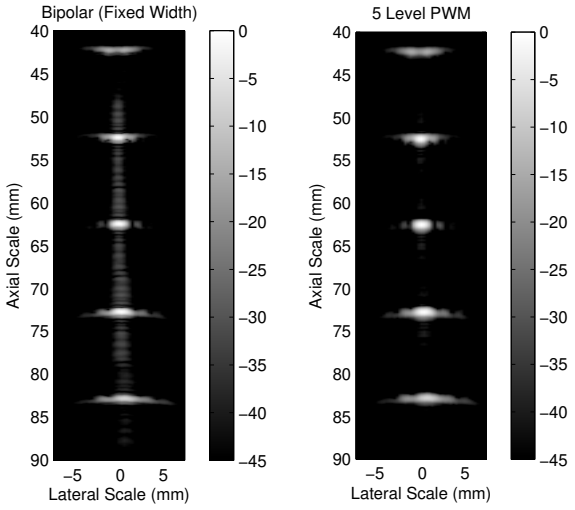

(a) (b)

Fig. 17. Experimental wire phantom coded images using the 'bipolar (fixed-width) pseudo-chirp' and PWM-encoded Hamming 3-6 MHz chirp signals.

which require transmitter amplitude control. The frequency

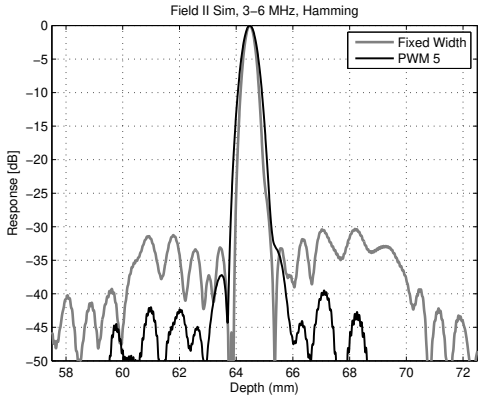

(a) Simulation

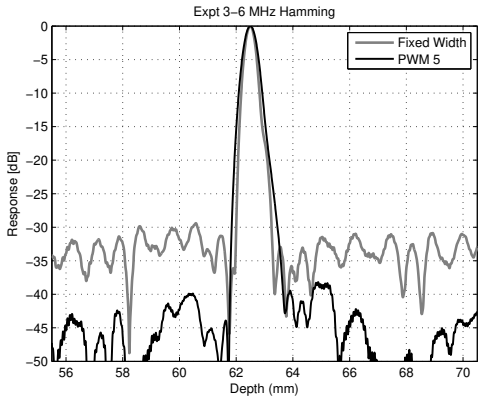

(b) Experimental

Fig. 18. Center line plotted limited to view a single wire at the focal point. Simulated data in Fig. 18(a). Experimentally obtained data in Fig. 18(b).

characteristics of the transducer causes filtering of harmonics within the square-wave, leaving the fundamental component. Modulation of square-wave pulses in accordance with this expected response enables the post-transducer pressure output to be accurately controlled. Section III demonstrated pressure control of arbitrary transmit sequences, with section IV demonstrating the potential benefit in LFM chirp coded imaging.

With respect to coded imaging, a number of other factors affect the performance of the system which have not been discussed in this work. These factors include the influence of the time-bandwidth product on the pulse-compressed output, additional windowing applied to the broadband chirp pulse by the transducer, and the effect of frequency dependent attenuation on the signal as it propagates in the medium. When considering the examples shown in this work, the cases shown are within, or at the limits of the transducer's reported bandwidth, and are suitable duration for coded imaging without causing severe overlapping in the time and frequency domains [31]. These restrictions cause the time-bandwidth product to be an order of magnitude lower than those found in coded radar [30] and thus restrict the gain improvement in SNR [17]. Due to the nature of the transducer's bandwidth, an additional tapering function will be applied to both signals. This can be viewed as useful, as increased tapering further reduces

sidelobes at a cost of widening the mainlobe. Also, as both signals are subject to the same level of transducer-induced tapering they are still directly comparable. All of these issues are discussed in more detail in the literature [16], [17] and [13]. With respect to the latter two issues, PWM techniques may be used to counteract for both the transducer bandwidth, and propagation by pre-distorting the waveform.

The described PWM method provides a best approximation of a desired waveform similar to that of commercial Digital to Analogue converters. Consequently, the waveform suffers from a certain amount of quantization based upon the number of PWM states available and the effect of comparing two discrete, sampled signals. The number of PWM states is dependent on the relationship between sampling frequency, and fundamental frequency, with a larger ratio between the two generating reduced quantization error. Additional error may also be introduced as a result of the carrier signal itself being a sampled signal. This can result in non-ideal carrier sampling, and consequently slight errors in the comparison method. The worst impact of which can be seen as anomalies in the PWM sequence in the form of missing or additional pulses. The advantage of the method when compared with other reported techniques such as Sigma-Delta modulation [22] is that arbitrary waveform sequences can be generated that operate at a fundamental mode, meaning that the frequency of switching, and hence power dissipation of front end components can be reduced.

Lastly, the sequences produced by the algorithm are actually MOSFET drive signals. These signals switch several MOSFETs between voltage states. As this is not an instantaneous transition it is therefore important to consider the rise and fall times of the MOSFET used, the characteristics of the load and any voltage drop across protection diodes to ensure maximum performance.

VII. Conclusions

Ultrasound array transducers are established transducer components, and require high-voltage excitation across multiple channels. A popular transmitter solution is the use of MOSFET devices operating in a 'switched-mode', selecting between a small number of discrete voltage levels. This has advantages over other 'analogue' excitation technologies, such as size and cost, however is reported to be restrictive in terms of arbitrary waveform capability and power control.

Several applications and areas exist throughout ultrasound that benefit from arbitrary waveform capability, or control of pressure output. Specific examples demonstrated in this work include arbitrary waveform generation and power control; apodization in imaging to reduce sidelobes and image artifacts; and generation of tapered, frequency-modulated, coded signals for use in coded imaging to increase SNR of weak scatterers. This work has presented a method of obtaining arbitrary waveform capability using a carrier-comparison, fundamental-mode, pulse-width modulation scheme that modulates widths according to the expected fundamental frequency component of a square-wave.

A carrier comparison method is a convenient strategy of encoding PWM sequences and is often used in many areas of engineering. We have shown that for ultrasound, a carrier comparison PWM method can successfully be used to control MOSFET devices common within most ultrasound systems, and offer amplitude control as an alternative to using DACs and linear power amplifiers. This has a number of advantages in terms of size, cost and potential device integration.

This paper discusses a number of ultrasound specific carrier modifications for generation of PWM sequences for ultrasound applications. These PWM sequences differ from 'traditional' PWM in a number of ways. Firstly, the carrier is modified so that widths are modulated according to the fundamental energy in the waveform as opposed to a linear carrier. Secondly, the carrier frequency is altered as to generate the least number of width-modulated pulses (single multi-level pulse per half cycle) necessary to describe the desired waveform. Thirdly, when used to encode frequency modulated signals, the same frequency modulation is applied to the carrier.

Acknowledgments

The authors would like to thank C. Vo Ky, B. Q. Bui, T. H. Pham, O. Anwar, P. Thompson, S. Qureshi and C. Winckler for their hard work on hardware and software development.

The authors would also like to thank Maxim Integrated Products and Texas Instruments for providing samples and GE Inspection Technologies for providing transducers.

References

[1] X. Xu, J. Yen, and K. Shung, "A low-cost bipolar pulse generator for high-frequency ultrasound applications," *Ultrasonics, Ferroelectrics and Frequency Control, IEEE Transactions on*, vol. 54, no. 2, pp. 443 –447, february 2007.

[2] C.-C. Huang, P.-Y. Lee, P.-Y. Chen, and T.-Y. Liu, "Design and implementation of a smartphone-based portable ultrasound pulsed-wave doppler device for blood flow measurement," *Ultrasonics, Ferroelectrics and Frequency Control, IEEE Transactions on*, vol. 59, no. 1, pp. 182 –188, january 2012.

[3] G.-D. Kim, C. Yoon, S.-B. Kye, Y. Lee, J. Kang, Y. Yoo, and T. kyong Song, "A single fpga-based portable ultrasound imaging system for point-of-care applications," *Ultrasonics, Ferroelectrics and Frequency Control, IEEE Transactions on*, vol. 59, no. 7, pp. 1386 –1394, july 2012.

[4] G. Athanasopoulos, S. Carey, and J. Hatfield, "Circuit design and simulation of a transmit beamforming asic for high-frequency ultrasonic imaging systems," *Ultrasonics, Ferroelectrics and Frequency Control, IEEE Transactions on*, vol. 58, no. 7, pp. 1320 –1331, july 2011.

[5] M. O'Donnell, "Coded excitation system for improving the penetration of real-time phased-array imaging systems," *Ultrasonics, Ferroelectrics and Frequency Control, IEEE Transactions on*, vol. 39, no. 3, pp. 341 –351, may 1992.

[6] M. Pollakowski and H. Ermert, "Chirp signal matching and signal power optimization in pulse-echo mode ultrasonic nondestructive testing," *Ultrasonics, Ferroelectrics and Frequency Control, IEEE Transactions on*, vol. 41, no. 5, pp. 655 –659, sept. 1994.

[7] J. Brown and G. Lockwood, "Low-cost, high-performance pulse generator for ultrasound imaging," *Ultrasonics, Ferroelectrics and Frequency Control, IEEE Transactions on*, vol. 49, no. 6, pp. 848 –851, june 2002.

[8] S. C. Tang and G. Clement, "A harmonic cancellation technique for an ultrasound transducer excited by a switched-mode power converter," *Ultrasonics, Ferroelectrics and Frequency Control, IEEE Transactions on*, vol. 55, no. 2, pp. 359 –367, february 2008.

[9] M. Urban, C. Chalek, R. Kinnick, T. Kinter, B. Haider, J. Greenleaf, K. Thomenius, and M. Fatemi, "Implementation of vibro-acoustography on a clinical ultrasound system," *Ultrasonics, Ferroelectrics and Frequency Control, IEEE Transactions on*, vol. 58, no. 6, pp. 1169 –1181, june 2011.

[10] Z. Gao and P. Gui, "A look-up-table digital predistortion technique for high-voltage power amplifiers in ultrasonic applications," *Ultrasonics, Ferroelectrics and Frequency Control, IEEE Transactions on*, vol. 59, no. 7, pp. 1550 –1557, july 2012.

[11] W. Qiu, Y. Yu, F. K. Tsang, and L. Sun, "A multifunctional, reconfigurable pulse generator for high-frequency ultrasound imaging," *Ultrasonics, Ferroelectrics and Frequency Control, IEEE Transactions on*, vol. 59, no. 7, pp. 1558 –1567, july 2012.

[12] K. Agbossou, J.-L. Dion, S. Carignan, M. Abdelkrim, and A. Cheriti, "Class d amplifier for a power piezoelectric load," *Ultrasonics, Ferroelectrics and Frequency Control, IEEE Transactions on*, vol. 47, no. 4, pp. 1036 –1041, jul 2000.

[13] R. S. Cobbold, *Foundations of Biomedical Ultrasound*. Oxford University Press, 2007.

[14] P. 't Hoen, "Aperture apodization to reduce the off-axis intensity of the pulsed-mode directivity function of linear arrays," *Ultrasonics*, vol. 20, no. 5, pp. 231–236, 1982.

[15] Y. Takeuchi, "An investigation of a spread energy method for medical ultrasound systems: Part one: Theory and investigation," *Ultrasonics*, vol. 17, no. 4, pp. 175 – 182, 1979.

[16] T. Misaridis and J. Jensen, "Use of modulated excitation signals in medical ultrasound. part i: basic concepts and expected benefits," *Ultrasonics, Ferroelectrics and Frequency Control, IEEE Transactions on*, vol. 52, no. 2, pp. 177 –191, feb. 2005.

[17] Misaridis, T. and Jensen, J.A., "Use of modulated excitation signals in medical ultrasound. part ii: design and performance for medical imaging applications," *Ultrasonics, Ferroelectrics and Frequency Control, IEEE Transactions on*, vol. 52, no. 2, pp. 192 –207, feb. 2005.

[18] T. Misaridis and J. Jensen, "Use of modulated excitation signals in medical ultrasound. part iii: high frame rate imaging," *Ultrasonics, Ferroelectrics and Frequency Control, IEEE Transactions on*, vol. 52, no. 2, pp. 208 –219, feb. 2005.

[19] H. W. Persson, "Electric excitation of ultrasound transducers for short pulse generation," *Ultrasound in Medicine & Biology*, vol. 7, no. 3, pp. 285 – 291, 1981.

[20] L. Franquelo, J. Rodriguez, J. Leon, S. Kouro, R. Portillo, and M. Prats, "The age of multilevel converters arrives," *Industrial Electronics Magazine, IEEE*, vol. 2, no. 2, pp. 28 –39, june 2008.

[21] B. D. Bedford and R. G. Hoft, *Principles of Inverter Circuits*. John Wiley & Sons, Inc., 1964.

[22] S.-W. Huang and P.-C. Li, "Arbitrary waveform coded excitation using bipolar square wave pulsers in medical ultrasound," *Ultrasonics, Ferroelectrics and Frequency Control, IEEE Transactions on*, vol. 53, no. 1, pp. 106 –116, jan. 2006.

[23] D. Holmes and T. Lipo, *Pulse Width Modulation for Power Converters: Principles and Practice*, M. E. El-Hawary, Ed. Wiley-IEEE Press, 2003.

[24] B. McGrath and D. Holmes, "Multicarrier pwm strategies for multilevel inverters," *Industrial Electronics, IEEE Transactions on*, vol. 49, no. 4, pp. 858 – 867, aug 2002.

[25] D. M. J. Cowell and S. Freear, "Quinary excitation method for pulse compression ultrasound measurements," *Ultrasonics*, vol. 48, pp. 98–108, 2008.

[26] P. R. Smith, D. M. J. Cowell, B. Raiton, C. Ky, and S. Freear, "Ultrasound array transmitter architecture with high timing resolution using embedded phase-locked loops," *Ultrasonics, Ferroelectrics and Frequency Control, IEEE Transactions on*, vol. 59, no. 1, pp. 40 –49, january 2012.

[27] F. Harris, "On the use of windows for harmonic analysis with the discrete fourier transform," *Proceedings of the IEEE*, vol. 66, no. 1, pp. 51 – 83, jan. 1978.

[28] A. Nuttall, "Some windows with very good sidelobe behavior," *Acoustics, Speech and Signal Processing, IEEE Transactions on*, vol. 29, no. 1, pp. 84 – 91, feb 1981.

[29] J. Adams, "A new optimal window," *Signal Processing, IEEE Transactions on*, vol. 39, no. 8, pp. 1753 –1769, aug 1991.

[30] C. E. Cook and M. Bernfeld, *Radar Signals*. Academic Press Inc., 1967.

[31] D. M. J. Cowell and S. Freear, "Separation of overlapping linear frequency modulated (lfm) signals using the fractional fourier transform," *Ultrasonics, Ferroelectrics and Frequency Control, IEEE Transactions on*, vol. 57, no. 10, pp. 2324 –2333, oct. 2010.

[32] J. A. Jensen, "Field: A program for simulating ultrasound systems," in *10th Noric Baltic Conference on Biomedical Imaging, Vol. 4, Supplement 1, Part 1:351–353*, 1996, pp. 351–353.

[33] J. Jensen, "Simulation of advanced ultrasound systems using field ii," in *Biomedical Imaging: Nano to Macro, 2004. IEEE International Symposium on*, 2004, pp. 636 – 639 Vol. 1.

Peter Smith received his B.Eng. (Hons) degree in Electronic Engineering (Industrial) and a M.Sc. degree in Embedded Systems Engineering from the University of Leeds, UK, in 2008 and 2009 respectively. As part of his undergraduate studies he completed a 12 month industrial placement working within Hardware Design Verification. His postgraduate M.Sc. project was the design of an 8-Channel FPGA-controlled Ultrasound Transmitter design. In 2009 he joined the Ultrasound Group within the School of Electronic and Electrical Engineering as a Ph.D. student. His main research interests include ultrasound instrumentation and system design, FPGA development, and ultrasound medical imaging.

David Cowell gained his doctorate from the School of Electronic and Electrical Engineering at the University of Leeds in 2008 working with the Ultrasound Group. His doctoral research area was advanced coding excitation techniques and excitation circuit design for industrial instrumentation and medical imaging systems. During this time he has performed extensive consultancy in instrumentation, FPGA and high-speed digital hardware design. After working as a research consultant in measurement and instrumentation, he joined the Ultrasound Group as a Research Fellow. His main research is currently focused on non-invasive industrial ultrasound measurement. His other active research areas include advanced miniaturized ultrasound excitation systems with low harmonic distortion for phased array imaging, ultrasound system design and signal processing.

Steven Freear (S'95, M'97, SM'11) gained his doctorate in 1997 and subsequently worked in the electronics industry for 7 years as a medical ultrasonic system designer. He was appointed Lecturer (Assistant Professor) and then Senior Lecturer (Associate Professor) in 2006 and 2008 respectively at the School of Electronic and Electrical Engineering at the University of Leeds. In 2006 he formed the Ultrasound Group specializing in both industrial and biomedical research. His main research interest is concerned with advanced analogue and digital signal processing and instrumentation for ultrasonic systems. He teaches digital signal processing, VLSI and embedded systems design, and hardware description languages at both undergraduate and postgraduate level. He has been Associate Editor for IEEE Transactions on Ultrasonics, Ferrorelectrics and Frequency Control since 2009, and was appointed Editor-In-Chief in 2013.